JOURNAL OF CATALYSIS 112, 168–175 (1988)

Oxidative Coupling of Methane over Antimony-Based Catalysts

M.-Y. LO, S. K. AGARWAL, AND G. MARCELIN[1]

Chemical and Petroleum Engineering Department, University of Pittsburgh, Pittsburgh, Pennsylvania 15261

Received October 20, 1987; revised February 8, 1988

The conversion of methane to C_2 hydrocarbons by oxidative coupling was studied using a series of potassium-doped bulk and supported antimony oxide catalysts over the temperature range 700–800°C. A combination of both pulse and flow reaction techniques was used in the study. The use of a tapered reactor design significantly reduced any gas-phase contribution to the reaction. α-Sb_2O_4 was identified as the only antimony oxide phase which gave high C_2 selectivity under the reaction conditions studied. It was found that addition of potassium to supported antimony oxide resulted in a slight increase in the C_2 yield and C_2 selectivity. Kinetic studies were used to elucidate the reaction mechanism.

INTRODUCTION

The surface catalyzed reaction of methane, leading to the formation of higher homologs, has not proven successful mainly because the direct coupling of methane is a thermodynamically prohibited process at temperatures and pressures of interest. If an oxidizing agent is present, however, either partial oxidation to methanol or oxidative coupling can take place. Recent work in a number of laboratories (*1–9*) has shown the feasibility of converting methane to higher homologs by reacting it with a metal oxide, thereby coupling the methane through the abstraction of lattice oxygen and the formation of water, i.e.,

$$xCH_4 + (x - 1)MO \rightarrow C_xH_{2x+2} + (x - 1)H_2O + (x - 1)M.$$

In addition to the oxidatively coupled products, such as ethane and ethylene, the oxidation of methane can result in total oxidation, leading to CO_2 and H_2O.

Early work by Union Carbide (*1*) focused on screening different metal oxides for the oxidative coupling of methane. Oxides of most of the low melting metals of IIIA, IVA, and VA were shown to exhibit both high activity and high selectivity for the coupling reaction. Other catalysts have been studied by different workers. For example, Sm_2O_3 has been reported to give C_2 selectivities as high as 93% (*10*), and PbO/MgO catalyst has been reported to give a C_2 selectivity of 87% (*11*). Sb_2O_4 was chosen in the present work as it lies in the low melting region of the periodic table and has been reported to give high C_2 selectivity (*1*). Additionally, Sb_2O_4 is a well-known allylic oxidation catalyst and has been reported to be a good coupling agent in propylene oxidation (*12*). This paper reports a study of the oxidation of methane, using potassium-modified antimony oxide catalysts, in an attempt to understand the reaction pathways leading to both the partial and the complete oxidation of methane.

EXPERIMENTAL

Catalyst Preparation

A series of potassium-doped antimony oxides was prepared by dissolving the acetate salts of potassium and antimony in a common solution and gently boiling it down, with constant stirring, to a paste. This was followed by drying at 120°C and calcining, first at 500°C for 15 h and then at 800°C for 4 h. Catalysts were prepared containing 0, 2.5, 5, 33, 50, and 66 at.% of potassium. Attempts to prepare catalysts containing approximately between 10 and 25

[1] To whom correspondence should be addressed.

0021-9517/88 $3.00

at.% K were unsuccessful since such compositions apparently fall within a "eutectic region" and would readily melt when subjected to the prescribed calcination treatment.

In addition to the bulk catalysts, Sb_2O_4 and 5% K–Sb_2O_4 supported on silica (Cab-O-Sil M5) were prepared using standard precipitation techniques. Sb_2O_3 was dissolved in concentrated hydrochloric acid and the solution added to the proper amount of support to give 17.3 wt% Sb loading. NH_4OH was used to precipitate Sb_2O_3 onto the support. The mixture was then stirred for 1 h at 70°C, filtered, and washed to remove Cl^- ions. In the case of potassium-doped antimony oxide, potassium carbonate was added to the Sb_2O_3/SiO_2 suspension. The suspension was heated until a thick paste remained, dried, and subjected to the described calcination treatment.

The BET surface area of the catalyst was determined by N_2 physisorption at −196°C using a Micromeritics 2600 system. X-ray diffraction (XRD) measurements were performed using a General Electric diffractometer with Cu$K\alpha$ radiation. Differential thermal analysis (DTA) curves to 1300°C were obtained using a Perkin–Elmer 1700 DTA at 5°C/min heating rate in flowing air.

Reaction Studies

The reaction was studied using a laboratory scale fixed-bed reactor system which could be operated in either a flow or a pulse mode. The reactor design is shown in Fig. 1. It consisted of a 7-mm-i.d. and 19-cm-length quartz tube fused onto a 1-mm-i.d. thick wall capillary quartz tube of approximately the same length and outside diameter. The "tapered" quartz junction corresponded to the middle of the heated zone and contained the catalyst which was held in place by a small plug of quartz wool. Approximately 15 cm of the 7-mm-i.d. tube served as a preheating zone. The reactor was heated in a tube furnace to reaction temperature and the temperature controlled

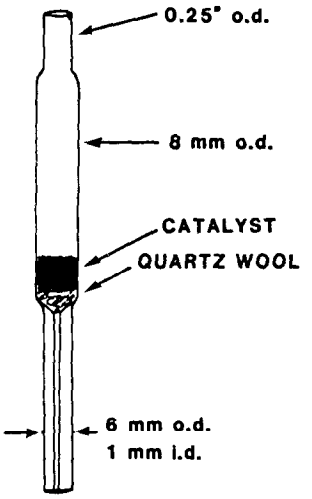

FIG. 1. Schematic diagram of tapered quartz reactor. Overall length is ca. 19 cm.

to ±1.0°C by a temperature controller (Omega Model CN-2010). In general, 200–1000 mg of catalyst was charged to the reactor in the form of 16/28 mesh pellets.

The gases methane (99.97%), oxygen (99.6%), and helium (99.995%) were further purified by passing through purifiers containing beds of indicating drierite and molecular sieves (5A). Flow rates were controlled by Tylan electronic mass flow controllers.

On-line analysis of the effluent gases was done using a gas chromatograph mounted with a TCD detector. The effluent gases were analyzed for methane, oxygen, carbon dioxide, carbon monoxide, ethylene, ethane, and water. The columns used were Porapak-Q and molecular sieves (5A). The calculations were carried out on the basis of total carbon atoms in the reactant gases. Product selectivity is defined as product yield divided by total methane conversion.

Although temperatures in the range 700 to 800°C were studied, most measurements were collected at 780°C, under pseudo-differential conditions (conversion less than 10%). In general, the partial pressures of the reactant gases, $CH_4/O_2/He$, were maintained in the ratio 9/2/7 at a total pressure

of approximately 1 atm. During flow experiments, the gas space velocity was maintained at 10,800 $cm^3/h/g$. For pulse experiments, a 0.5-ml sample of either methane : helium (9 : 7) or methane : oxygen : helium (9 : 2 : 7) was pulsed into the catalyst bed and directed to the gas chromatograph for analysis. A flow rate of 30 ml/min was used in the pulse experiments. At least 15 min elapsed between subsequent pulses.

TABLE 1

Characteristics of Antimony Catalysts

Catalyst	BET surface area (m^2/g)	Predominant phases (by XRD)
Sb_2O_4	4.1	α-Sb_2O_4
2.5% K–Sb	1.2	α-Sb_2O_4
5% K–Sb	3.6	Amorphous
33% K–Sb	0.9	Sb_6O_{13}
50% K–Sb	1.2	$KSbO_3$, K_2O
66% K–Sb	1.0	$KSbO_3$, K_2O
Sb/SiO_2	129.0	α-Sb_2O_4
5% K–Sb/SiO_2	116.0	α-Sb_2O_4

RESULTS

Because of the relatively high temperature necessary in affecting the methane coupling reaction, the role of gas-phase reaction must be understood. The importance of gas-phase reaction was tested by performing a series of blank experiments, i.e., in the absence of catalyst, in the flow mode. These results are shown in Fig. 2 for two types of reactor designs, the tapered reactor used in these studies, and a straight 7-mm-i.d. tube. Total methane conversion, using the tapered reactor, was less than 0.2% at temperatures up to 800°C. In contrast, when the straight tube reactor is used, a one order of magnitude increase in methane conversion was observed.

It is likely that the tapered reactor design allows for the rapid removal and quenching of effluent gases from the catalyst bed. This, in turn, reduces significantly any gas-phase contribution to the reaction. As a result, the tapered reactor design was used in all subsequent experiments.

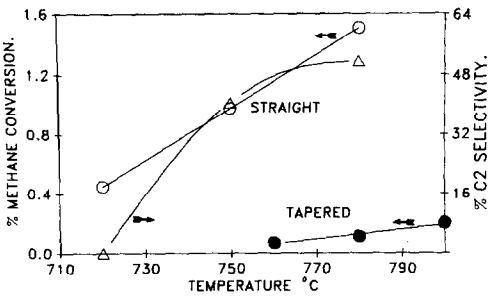

FIG. 2. Effect of reactor shape on reaction in the absence of catalyst. Tapered reactor gives 100% C_2 selectivity.

BET surface area measurements, XRD, and DTA of the catalysts were routinely performed. BET surface area and XRD results for the different catalysts are shown in Table 1. X-ray diffraction analysis revealed all the materials but one to be highly crystalline, consisting of mixed phases, such as Sb_2O_4, K_2O, and $KSbO_3$. Only the 5% K–Sb was found to be almost entirely amorphous to XRD. Additionally, its composition falls just outside the observed eutectic region. One can speculate that at this composition the metal oxides are in the state of a solid solution, resulting in a high degree of mixing of the two components. The presence of α-Sb_2O_4 phase in the catalysts was further confirmed by performing DTA of the catalyst in air medium which showed an endothermic peak at 1150°C corresponding to the conversion of α- to β-Sb_2O_4. It should be noted that the presence of potassium, unlike MoO_3 (*13*), did not affect the $\alpha \rightarrow \beta$ transition in Sb_2O_4.

Table 2 summarizes the catalytic behavior of both the bulk and the supported materials. In agreement with previous published results, bulk antimony oxide was found to exhibit good selectivity for the oxidative coupling products (*1*). However, as shown in Fig. 3A, rapid deactivation of the catalyst took place, with methane conversion dropping to less than one-half of its initial value in 3 h. The addition of potassium induced changes in the reaction, resulting in

TABLE 2

Catalytic Properties of Antimony-Based Materials for the Oxidative Coupling of Methane at 780°C

	Methane conversion (%)	C_2 yield (%)	Selectivities		
			C_2	CO	CO_2
Sb_2O_4	3.7	2.0	55	24	21
2.5% K–Sb	3.5	1.4	40	21	39
5% K–Sb	4.9	2.5	52	16	32
33% K–Sb	8.8	1.4	16	2	82
50% K–Sb	8.3	0.6	7	6	87
66% K–Sb	7.5	2.3	30	0	70
Sb/SiO_2	3.8	1.8	48	23	27
5% K–Sb/SiO_2	4.3	2.5	57	23	20

an increase in catalyst stability which appears to be related to the amount of potassium present. Figure 3B shows the change in product yield as a function of time for the bulk Sb_2O_4 catalyst. It should be noted that most of the observed deactivation in the overall conversion can be attributed to a decrease in CO_x yield. The total amount of C_2 products was observed to decrease only slightly with reaction time.

An increase in the amount of potassium to beyond the eutectic region resulted in an abrupt change in catalytic behavior. Thus 33% K–Sb showed high catalyst stability but poor C_2 selectivity. Addition of 50% K to Sb results in the formation of potassium antimonate phases giving very low C_2 selectivity. The slight increase in C_2 selectivity beyond 50% K–Sb may be attributed to the K_2O phase. Although it is difficult to compare yields because of the variation in surface areas among the catalysts, it is interesting to note that in spite of the large changes in activity and selectivity observed upon addition of potassium, the total C_2 yield (conversion times selectivity) remained approximately constant in all catalysts.

Figure 4 shows the effect of temperature on the methane conversion and the selectivities of the various products of interest for the 5% K–Sb catalyst. In the range of temperatures studied, a close correlation was found between the selectivity for coupled products and the overall methane conversion, whereas the reverse trend was observed for CO_2 selectivity. Similar results were observed for other K–Sb compositions.

Power rate laws of the form

$$d(\text{product})/dt = k(CH_4)^n(O_2)^m$$

were determined for the formation of the two principal products, ethane and CO_2, as models for partial vs total oxidation. These power rate law parameters for the different catalysts are shown in Table 3.

The effect of feed oxygen was investigated by performing the reaction in a pulse mode and using both methane–oxygen mixtures and pure methane reactants. Figure 5 shows the typical product distribution obtained in the pulse mode over Sb/SiO_2 catalyst. In the absence of molecular oxygen,

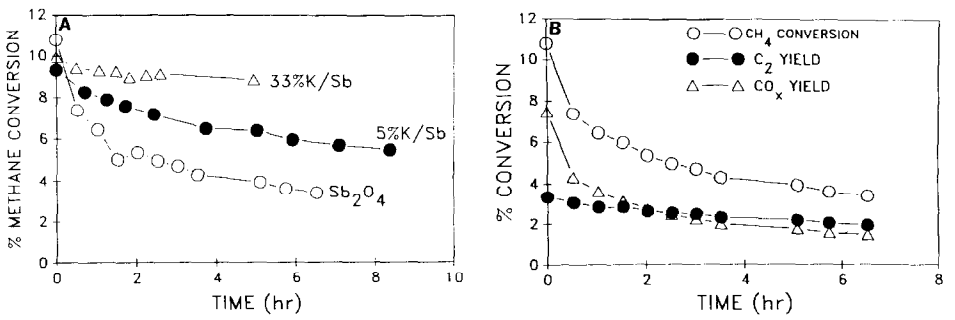

FIG. 3. Time dependence on methane coupling reaction at 780°C. (A) Total methane conversion; (B) product selectivity using α-Sb_2O_4 (bulk) catalyst.

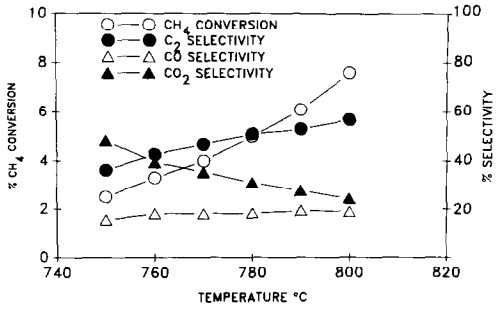

FIG. 4. Effect of temperature on reaction selectivity. Catalyst represented is bulk 5% K–Sb.

TABLE 3

Kinetic Parameters for Methane Oxidation

Catalyst	$R_{C_2} = k[O_2]^m[CH_4]^n$			$R_{CO_2} = k'[O_2]^m[CH_4]^n$		
	E_a (kcal/mol)	m	n	E_a (kcal/mol)	m	n
Sb_2O_4	56.0	0.5	0.9	22.8	0.8	0.4
5% K–Sb	62.0	0.2	0.6	23.0	0.8	0.1
33% K–Sb	62.0	1.0	1.1	30.8	1.0	0.2
Sb–SiO_2	56.1	0.7	0.8	40.2	0.7	0
5% K–Sb/SiO_2	70.0	0.4	1.0	38.5	0.5	0.5
K–Bi_2O_3/Al_2O_3[6]	—	1	2	—	1	0.3
Na–PbO/Al_2O_3[7]	—	1.1	0.8	—	1.5	0.4

consecutive methane pulses caused an immediate decrease in both the ethane and the CO_2 yields, with the latter decreasing to almost zero after only three pulses. The ethane yield was observed to decrease rapidly after the first pulse and to reach steady state after five pulses. It should be noted that at this point, and in the absence of O_2, the selectivity to C_2 products approached 100%.

When the reactant mixture was switched to methane : oxygen (9 : 2), the CO_2 yield immediately increased to almost twice its initial value. The C_2 yield also increased, but to less than its initial value. No changes in conversion or selectivity were observed with subsequent pulses. Changing the reactant feed back to pure methane returned the yields to their previous steady-state values.

DISCUSSION

Predominantly three different antimony phases, α-Sb_2O_4, Sb_6O_{13}, and $KSbO_3$, were identified in the different catalysts studied. Of these, only α-Sb_2O_4 was found to give high C_2 selectivity. As seen from Table 1, the presence of Sb_6O_{13} or $KSbO_3$ decreased the C_2 selectivity significantly.

Although the 5% K–Sb catalyst was shown amorphous by XRD, when calcined at 945°C, it showed the presence of α-Sb_2O_4 phase. In addition, the DTA pattern showed an exotherm at the characteristic $\alpha \rightarrow \beta$-Sb_2O_4 transition temperature, indicating the presence of the α-form. It is believed that the amorphous nature of the catalyst calcined at 800°C may be simply due to a poorly developed crystal structure.

The addition of small amounts of potassium (<5%) appeared to have little effect in the steady-state catalytic behavior of either the bulk or the supported materials. At high levels of potassium (>33%), significant changes in the activities and selectivities were observed. It should be noted, though, that any decrease in C_2 selectivity observed upon addition of potassium was typically accompanied by an increase in the overall activity. Thus, the addition of potassium only affected the relative product selectivities and made little difference in the observed C_2 yields. Similarly, the observed changes in overall activity with time were primarily due to changes in the CO_x yield. This behavior was observed in all the cata-

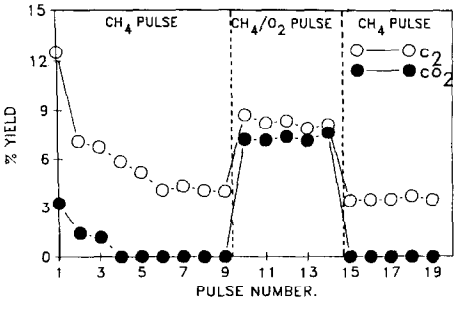

FIG. 5. Product distribution in pulsed conversion of methane over Sb/SiO_2. Amount injected in each pulse is 0.5 ml.

lysts studied and appeared to be independent of catalyst composition and initial activity.

This type of behavior suggests that excess amounts of potassium can result in the formation of certain antimonate compounds which lead predominately to the total oxidation products, and that two parallel routes may occur on some of these catalysts, one route leading to C_2 products and the other leading to CO_x. It is, of course, dangerous to make highly quantitative comparisons across the catalysts since there are many variances, such as surface area and preparation which can not be fully taken into account.

The carbon dioxide produced during the oxidative coupling of methane may be formed directly from methane, from methane-like intermediates, or from product hydrocarbons. Both the power rate law and the activation energies for the formation of ethane and CO_2 were quite different for the catalysts studied, suggesting different reaction paths, or at least different rate-determining steps. The difference in the measured activation energies, the linearity of the Arrhenius plot within the temperature range studied, and the temperature dependence of the ethane and CO_2 selectivities suggest that the CO_2 is not a secondary product from C_2, but it is formed directly from methane. It should be noted that this lack of secondary oxidation reactions is a function of methane conversion and at higher temperatures, significant production of CO_2 from ethane can be expected.

The measured values for the activation energy for ethane formation agree well with published results for other catalyst systems (*14, 15*). Its relatively high value is consistent with a hydrogen abstraction step being rate determining. For the Mg–Li system, Lunsford and co-workers (*8*) have suggested a mechanism in which the active sites on the catalyst surface are $[Li^+O^-]$ centers. Although we have no direct evidence, it is likely that the coupling mechanism over antimony oxide is the same as that proposed for Li–Mg, Na–Mn, and other catalysts (*15, 16*): mainly, hydrogen abstraction from methane, desorption of methyl radicals into the gas phase, and gas-phase coupling of the methyl radicals to form ethane. The complex and varied oxygen dependence measured for the formation of partial oxidation products is typical of reactions involving a reduction–oxidation cycle of the catalyst and agrees well with values reported for other catalyst systems (*17, 18*).

The mechanism leading to the formation of the carbon oxides has received relatively little attention in the literature. The vast difference in activation energies between CO_2 and C_2H_6 formation would at first suggest that methyl radicals are not involved in CO_2 formation, and that total oxidation products are formed independently of the methyl radicals leading to coupling products. However, the formation of an *unstable* intermediate following the formation of gas-phase methyl radicals can also account for such results. For example, a methyl radical could react with gas-phase oxygen to form an unstable methylperoxy radical which could decompose to a carbon oxide:

$$CH_3\cdot + O_2 \leftrightharpoons CH_3O_2\cdot \rightarrow CO_x$$

The same argument can be used with unstable intermediate adsorbed species:

$$CH_3\cdot + O(s) \leftrightharpoons CH_3O(s) \rightarrow CO_x$$

Such equilibria would shift to the left with increasing temperatures, leading to an apparent activation energy which would be smaller than the activation energy for the rate-determining step, i.e., hydrogen abstraction. The existence of methylperoxy radicals was argued by Lunsford and coworkers to account for the observed behavior of selectivity with temperature (*15*). It should be noted, however, that although methyl radicals have been isolated and successfully identified using ESR techniques during methane coupling, no similar report exist concerning the identification of methylperoxy radicals. This may be due, in

part, to their relative instability making detection difficult.

The pulse experiments over Sb/SiO_2 indicate that different oxygen species are responsible for CO_2 and ethane formation. The negligible CO_2 yield observed after the fourth methane pulse suggests that CO_2 may be formed from an oxygen species which is rapidly consumed in the first three methane pulses. The sharp increase in CO_2 yield which is observed when a combination of CH_4 and O_2 is pulsed can be attributed to gas-phase reaction or to weakly adsorbed oxygen. Brown and Patterson have reported that, for antimony–tin catalysts, adsorbed oxygen is highly selective for total methane oxidation (*19*). The achievement of a steady state C_2 yield with pure methane feed and the extremely high C_2 selectivity indicates that lattice oxygen is involved primarily in C_2 production.

Based on these results, it can be postulated that there are multiple pathways in the oxidative reaction of methane over antimony oxide catalysts. These are summarized in Fig. 6. The oxidative coupling route over these catalysts is proposed to proceed, as in other catalytic systems, by abstraction of hydrogen by lattice oxygen and gas-phase coupling of methyl radicals. This pathway can be maximized by operating in the absence of molecular oxygen.

The pathways leading to complete oxidation are more complex. The high CO_2 selectivity observed when the reaction is conducted in the presence of molecular oxygen indicates a significant gas-phase contribution to CO_x production, perhaps via methylperoxy radicals, or possibly through adsorbed molecular oxygen. In addition, there is a non-gas-phase route, i.e., surface-assisted, evident during the initial phases of reaction in the absence of molecular oxygen, which also contributes to CO_x production. This could be caused either by reaction of methyl radical with surface species or by a direct pathway from methane. This work cannot differentiate between these two possibilities. A noncatalytic route is also possible, as was shown in the blank experiments, but this can be minimized by appropriate experimental design.

Finally, the role of potassium must be examined. It has been proposed that the presence of acidic sites on the catalyst surface leads to nonselective oxidation (*7*). It has also been claimed that addition of alkali decreases the nonselective oxidation by neutralizing the acidic sites. However, in the present study, it has been found that addition of large amounts of potassium to antimony oxide catalysts reduces that C_2 selectivity. This is probably due to the formation of distinct Sb_6O_{13} and $KSbO_3$ phases which are primarily CO_2 producers.

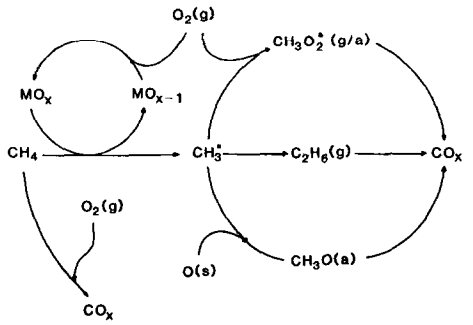

FIG. 6. Reaction scheme for the oxidative coupling of methane.

ACKNOWLEDGMENT

The financial support of the Gas Research Institute is gratefully acknowledged.

REFERENCES

1. Keller, G. E., and Bhasin, M. M., *J. Catal.* **73,** 9 (1982).
2. U.S. Patent 4,443,644 (1984).
3. U.S. Patent 4,443,645 (1984).
4. U.S. Patent 4,443,646 (1984).
5. U.S. Patent 4,443,647 (1984).
6. Ali Emesh, I. T., and Amenomiya, Y., *J. Phys. Chem.* **90,** 4785 (1986).
7. Hinsen, W., Bytyn, W., and Baerns, M., "Proceedings, 8th International Congress on Catalysis, Berlin, 1984," Vol. III, p. 581. Dechema, Frankfurt-am-Main, 1984.

8. Driscoll, J., Martir, W., Wang, J. X., and Lunsford, J. H., *J. Amer. Chem. Soc.* **107,** 58 (1985).
9. Ito, T., and Lunsford, J. H., *Nature (London)* **314,** 721 (1985).
10. Otsuka, K., Jinno, K., Morikawa, A., *J. Catal.* **100,** 353 (1986).
11. Asami, K., Hashimoto, S., Shikada, T., Fujimoto, K., and Tominaga, H. O., *Chem. Lett.,* 1233 (1986).
12. Fattore, V., Fuhrman, Z. A., Manara, G., and Notari, B., *J. Catal.* **37,** 215 (1975).
13. Teller, R. G., Antonio, M. R., Brazdil, J. F., Mehicic, M., and Grasseli, R. K., *Inorg. Chem.* **24,** 3370 (1985).
14. Kimble, J. B., and Kolts, J. H., *Energy Prog.* **6,** 226 (1987).
15. Ito, T., Wang, J. X., Lin, C. H., and Lunsford, J. H., *J. Amer. Chem. Soc.* **107,** 5062 (1985).
16. Jones, C. A., Leonard, J. J., and Sofranko, J. A., *J. Catal.* **103,** 311 (1987).
17. Thomas, J. M., and Thomas, W. J., "Introduction to the Principles of Heterogeneous Catalysis." Academic Press, San Diego/London, 1967.
18. Bartek, J. P., Hupp, J. M., Brazdil, J. F., and Grasselli, R. K., *Prepr. Amer. Chem. Soc. Div. Pet. Chem.* **33,** 774 (1987).
19. Brown, I., and Patterson, W. R., *J. Chem. Soc. Faraday Trans. 1* **79,** 1431 (1983).